Radiative emission and energy deposition in transient luminous events

2008 J. Phys. D: Appl. Phys. 41 234014

(http://iopscience.iop.org/0022-3727/41/23/234014)

J. Phys. D: Appl. Phys. **41** (2008) 234014 (14pp) doi:10.1088/0022-3727/41/23/234014

Radiative emission and energy deposition in transient luminous events

C L Kuo[1,2], A B Chen[2], J K Chou[2], L Y Tsai[2], R R Hsu[2], H T Su[2], H U Frey[3], S B Mende[3], Y Takahashi[4] and L C Lee[1]

[1] Institute of Space Science, National Central University, Jhongli, Taiwan
[2] Department of Physics, National Cheng Kung University, Tainan, Taiwan
[3] Space Sciences Laboratory, University of California, Berkeley, California, USA
[4] Department of Geophysics, Tohoku University, Sendai, Japan

E-mail: clkuo@jupiter.ss.ncu.edu.tw

Received 31 March 2008, in final form 6 August 2008
Published 20 November 2008
Online at stacks.iop.org/JPhysD/41/234014

Abstract
The Imager of Sprites and Upper Atmospheric Lightning (ISUAL) experiment on the FORMOSAT-2 satellite has recently reported that an elve is the most dominant type of transient luminous events (TLEs) and deduced the global occurrence rates of sprites, halos and elves to be ∼1, ∼1 and 35 events/min, respectively (Chen *et al* 2008 *J. Geophys. Res.* **113** A08306). In this paper, we report the computed radiative emission and energy precipitation of the TLEs in the upper atmosphere. By analysing 1415 ISUAL TLEs, we found that for sprites, halos and elves the spatially averaged brightness are 1.5, 0.3 and 0.17 MR, and the energy deposition is 22, 14 and 19 MJ per event. After factoring in the global occurrence rates, the global energy deposition rates in the upper atmosphere are 22, 14 and 665 MJ min^{-1} from sprites, halos and elves.

1. Introduction

In the past two decades, thunderstorms have been found to be capable of inducing upper atmospheric flashes now carrying the names of sprites [1], elves [2, 3], halos [4, 5], blue jets [6, 7] and gigantic jets (GJs) [8, 9]. Luminous structures of these transient luminous events (TLEs) range from the metre-scale to the kilometre-scale and even span the region from the cloud top to the lower ionosphere as in the case of a GJ.

Sprites are fleeting luminous columns at altitudes of 40–90 km above very active thunderstorms, and their lateral spread ranges from several to tens of kilometres [1]. Sprites are mostly induced by the quasi-static electric field established by positive cloud-to-ground (CG) lightning discharges. The time delays between the lightning return stroke and the sprite initiation are several to hundreds of milliseconds [10]. The luminous duration of sprites lasts from several to tens of milliseconds (ms). The typical brightness of sprites is several to tens of mega-Rayleigh (MR) [5, 11]. Recently, a 10 000 fps observation showed that the brightness can be up to 1 giga-Rayleigh (GR) [12] at the streamer head of sprites.

Elves have a very short luminous duration (hundreds of microseconds to 1 ms). Hence they are very hard to identify in ground observations. Elves occur near the airglow layer altitude (∼80–95 km) with a lateral dimension of ∼200–500 km. The typical brightness of elves as reported by a space-borne instrument is hundreds of kR at the exposure time of 14 or 29 ms [13, 14]. The estimated peak brightness for $1PN_2$ at the time-integrated time of 0.1 ms can be up to 44 MR [14]. Elves are induced by the electromagnetic pulse (EMP) radiated by the CG lightning discharges. A typical CG lightning will radiate 1–10 GJ of energy [15]. Although most of the radiated electromagnetic energy reflects from the bottom of the ionosphere, a small fraction of the EMP energy dissipates in the lower ionosphere and produces the elves. Ground observations have shown that CG lightning with peak currents exceeding 57 kA will always generate elves [16].

A halo is a brief and diffuse pancake-shaped TLE at ∼70–85 km altitude with a diameter of less than 100 km [4, 17], which is substantially smaller than an elve. Moreover, the luminous disc of a halo has a straight upper edge and a curvy lower edge that clearly distinguishes it from elves. The generating mechanism for halos is the same as that for sprites—initiated by the lightning-induced quasi-static electric field between the cloud and the lower ionosphere. Hence halos often precede sprites but could also occur alone.

GJs have the largest luminous structure among the TLEs. They can span the whole altitude range from the cloud top at ∼15 km to the lower ionosphere at ∼90 km as reported by several ground campaigns [6, 8, 9] and a satellite observation

[18]. Based on black/white NTSC video images, the optical evolution of GJs contains three stages: the leading jet, the fully developed jet and the trailing jet [8]. The leading jet is the pre-stage of the fully developed jet and its propagating behaviour is similar to a stepped leader in conventional lightning. At the fully developed stage, the morphology of GJs is a hybrid between sprites and blue jets. The trailing jet has similar features to those of a blue jet and emerges from the cloud top up to ∼60 km altitude. The optical emission of a trailing jet often lasts longer than 300 ms. The whole luminous period of GJs is ∼0.5 s.

Sprite spectra have been measured from the ground using filtered photometry [19, 20] and ICCD spectrographs [21–24]. The major emissions include the nitrogen first positive ($1PN_2$), second positive ($2PN_2$) and first negative bands ($1NN_2^+$). Based on a numerical simulation, Liu and Pasko [25] predicted that the nitrogen LBH band should also exist in sprite emission. Almost in no time, LBH emission was confirmed in ISUAL recorded sprites and elves [14, 26, 27]. In this paper, we consider only major emission bands of molecular nitrogen: $1PN_2$, $2PN_2$, LBH N_2 and $1NN_2^+$; since the emission from oxygen is relatively weak compared with molecular nitrogen as will be shown in section 3.1.

TLEs are optical manifestations of the coupling between the troposphere and the upper atmosphere. The radiative emission is the result of the transfer of tropospheric energy in the upper atmosphere. The discovery of TLEs in the upper atmosphere not only provided the direct evidence on the electrodynamical coupling between thunderstorms in the troposphere and the upper atmosphere, but also calls for our attention to their environmental impacts [28] and their role in the Earth's global electrical circuit [29]. One important way to elucidate the role of TLEs in the Earth's environment is to learn the energy deposited by them.

For the chemical kinetics associated with the air breakdown process in the sprite streamer at 70 km altitude, Sentman *et al* [30] have considered detailed chemical reactions in the electric-field driven processes, the follow-on chemistry, and the afterglow of the trailing region. In the initial phase of a sprite event, electrons accelerated by local E-field in the streamer tip can excite or even ionize molecular nitrogen and molecular oxygen. The total energy deposition in a TLE includes the electron impact energy transfer to molecular nitrogen and oxygen, the energy in forming minor species and the energy in other chemistry reactions. In this paper, we focus on the initial phase of electric-field driven processes and derive the energy deposition based on the energy transfer to atmospheric major species, N_2 and O_2. As will be demonstrated in section 3, this energy can be derived from the optical emissions of TLEs. However, the assessment of energy deposition in TLEs needs to be revised if the energy release through the formation of minor species and other chemical reactions are later found to be greater than that in the electric-field driven electron impact processes.

This paper is organized as follows. In section 2, the FORMOSAT-2 (FS-2) satellite and ISUAL payload are introduced. In section 3, we utilize an electrical field driven kinetic model involving electron impact processes of 39 reactions as listed in tables 1 and 2 for molecular nitrogen (78.1%) and oxygen (20.9%). From the model calculations, we derive the ratio of the total energy deposition in the radiative processes to that in the $1PN_2$ band of TLEs. The energy in the $1PN_2$ band is defined as the total excited number (occupation number) of the $1PN_2$ band multiplied by the threshold electron energy needed to excite this band. To deduce the total excited number in the $1PN_2$ band, we compute the theoretical spectra of TLEs, take the quenching effect that de-excites the excited N_2 into account, and correct for the photon absorption and scattering along the path between TLE and FS-2. After all the reducing effects that could affect the observations are corrected, a reliable total excited number in the $1PN_2$ band of TLEs can be extracted. In section 4, we demonstrate how to apply the procedures developed in section 3 to the ISUAL recorded sprites, halos, elves and GJs. In all, we analysed 1415 ISUAL TLEs to obtain the average brightness of sprites, halos and elves. From the derived excited number in the $1PN_2$ band, the total energy deposition in TLEs based on the ISUAL optical emission data can be inferred. In section 5, we discuss the possible magnitude of energy associated with the other chemical reactions in TLEs and the lightning energy contribution to the upper atmosphere. The main results of this work are summarized in section 6.

2. Instrument and observation

ISUAL is the first satellite experiment dedicated to a long-term global survey of TLEs [31]. The ISUAL payload is mounted on a sun-synchronous satellite—FS-2, which features 14 daily revisiting-orbits and has a designed life of five years. ISUAL has successfully entered the on-orbit observation phase after 1 July 2004. As of the end of 2007, more than 8000 TLEs have been recorded [32].

The ISUAL payload contains three sensor packages: a filter-wheel equipped intensified CCD imager, a six-channel spectrophotometer (SP) and a dual-band array photometer (AP). For the TLEs reported in this paper, the imager data were recorded through the 623–750 nm $1PN_2$ filter and with an image frame integration time of 29 ms. The ISUAL SP consists of six bandpass-filtered PMTs that cover the major emission bands of nitrogen. The bandpass selections are SP1 (150–290 nm; FUV; N_2 LBH band), SP2 (centred at 337 nm with a bandwidth 5.6 nm; for $2PN_2(0–0)$), SP3 (centred at 391.4 nm with a bandwidth 4.2 nm; for $1NN_2^+(0–0)$), SP4 (608.9–753.4 nm; for the $1PN_2$ band), SP5 (centred at 777.4 nm; for lightning O I emission) and SP6 (228.2–410.2 nm; for the $2PN_2$ band). The SP passing bands and their relation to the molecular nitrogen emission bands are shown in figure 3. The ISUAL AP contains a blue (370–450 nm) and a red (530–650 nm) array. Each array has 16 vertically stacked PMTs that provide temporal and spatial variations of emissions along the vertical direction [33]. On trigger, the ISUAL imager snaps six frames of images (1 frame before the trigger and 5 frames after), SP samples at a constant rate of 10 kHz for 205 ms and the AP samples at a rate of 20 kHz for the first 20 ms then slows down to 2 kHz for a total length of 240 ms.

Table 1. Inelastic collisions of electrons with molecular nitrogen.

Collision process	Reaction	Threshold energy (eV)	Reaction #
N_2 rotational	$e + N_2 \rightarrow e + N_2(\text{rotational})$	0.02	R1
N_2 vibrational	$e + N_2 \rightarrow e + N_2(v = 1)$	0.29	R2
	$e + N_2 \rightarrow e + N_2(v = 1)$	0.291	R3
	$e + N_2 \rightarrow e + N_2(v = 2)$	0.590	R4
	$e + N_2 \rightarrow e + N_2(v = 3)$	0.88	R5
	$e + N_2 \rightarrow e + N_2(v = 4)$	1.17	R6
	$e + N_2 \rightarrow e + N_2(v = 5)$	1.47	R7
	$e + N_2 \rightarrow e + N_2(v = 6)$	1.76	R8
	$e + N_2 \rightarrow e + N_2(v = 7)$	2.06	R9
	$e + N_2 \rightarrow e + N_2(v = 8)$	2.35	R10
N_2 electronic	$e + N_2 \rightarrow e + N_2(A\,^3\Sigma_u^+, v = 1\text{–}4)$	6.17	R11
	$e + N_2 \rightarrow e + N_2(A\,^3\Sigma_u^+, v = 5\text{–}9)$	7.00	R12
	$e + N_2 \rightarrow e + N_2(B\,^3\Pi_g)$ [1PN$_2$]	7.35	R13
	$e + N_2 \rightarrow e + N_2(W\,^3\Delta_u)$	7.36	R14
	$e + N_2 \rightarrow e + N_2(A\,^3\Sigma_u^+, v = 10-)$	7.80	R15
	$e + N_2 \rightarrow e + N_2(B'\,^3\Sigma_u^-)$	8.16	R16
	$e + N_2 \rightarrow e + N_2(a'\,^1\Sigma_u^-)$	8.40	R17
	$e + N_2 \rightarrow e + N_2(a\,^1\Pi_g)$ [LBH N$_2$]	8.55	R18
	$e + N_2 \rightarrow e + N_2(w\,^1\Delta_u)$	8.89	R19
	$e + N_2 \rightarrow e + N_2(C\,^3\Pi_u)$ [2PN$_2$]	11.03	R20
	$e + N_2 \rightarrow e + N_2(E\,^3\Sigma_g^+)$	11.88	R21
	$e + N_2 \rightarrow e + N_2(a''\,^1\Sigma_g^+)$	11.25	R22
N_2 sum of singlet states	$e + N_2 \rightarrow e + N_2^*$	13.00	R23
N_2 ionization	$e + N_2 \rightarrow 2e + N_2^+(X\,^2\Sigma_g^+, A\,^2\Pi_u)$	15.6	R24
	$e + N_2 \rightarrow 2e + N_2^+(B\,^2\Sigma_u^+)$ [1NN$_2^+$]	18.8	R25

Table 2. Inelastic collisions of electrons with molecular oxygen.

Collision process	Reaction	Threshold energy (eV)	Reaction #
O_2 rotational	$e + O_2 \rightarrow e + O_2(\text{rotational})$	0.02	R26
O_2 vibrational	$e + O_2 \rightarrow e + O_2(v = 1)$	0.19	R27
	$e + O_2 \rightarrow e + O_2(v = 2)$	0.38	R28
	$e + O_2 \rightarrow e + O_2(v = 3)$	0.57	R29
	$e + O_2 \rightarrow e + O_2(v = 4)$	0.75	R30
O_2 electronic	$e + O_2 \rightarrow e + O_2(a\,^1\Delta_g)$	0.977	R31
	$e + O_2 \rightarrow e + O_2(b\,^1\Sigma_g^+)$	1.627	R32
	$e + O_2 \rightarrow e + O_2(c\,^1\Sigma_u^-)$	4.50	R33
O_2 dissociation	$e + O_2 \rightarrow e + O(^3P) + O(^3P)$	6.00	R34
	$e + O_2 \rightarrow e + O(^3P) + O(^1D)$	8.40	R35
	$e + O_2 \rightarrow e + O(^1D) + O(^1D)$	10.00	R36
	$e + O_2 \rightarrow e + O(^3P) + O(^3S^0)$	14.7	R37
O_2 ionization	$e + O_2 \rightarrow 2e + O_2^+(X\,^2\Pi_g)$	12.06	R38
O_2 two-body attachment	$e + O_2 \rightarrow e + O_2^-$	——	R39

In the night hemisphere of the Earth, the FS-2 satellite treks from the South Pole to the North Pole and ISUAL is configured to view eastwards towards the local pre-midnight area. The ISUAL imager, SP and AP are all co-aligned at the centre of their views. The ISUAL imager and SP have the same field-of-view (FOV) of 20° (horizontal) × 5° (vertical). The combined FOV of each AP module is 22° (H) × 3.6° (V) [33]. The ISUAL imager observes an area of nearly three million square kilometres of Earth's surface with a near edge at a distance of 2370 km and a far edge of 4400 km [31, 33].

3. Data analysis

The occurrence of TLEs, including sprites, halos and elves, are often attributed to the quasi-static electrical field or the EMP radiated by the underlying thunderstorms. Moreover, the Earth atmosphere also often contains a minute amount of free electrons from cosmic ray bombardments or other ionization sources. In the case of sprite, if the lightning-induced electric-field strength exceeds the conventional breakdown value (E_k; [34, pp 135–6]), the ambient electron cloud could develop into

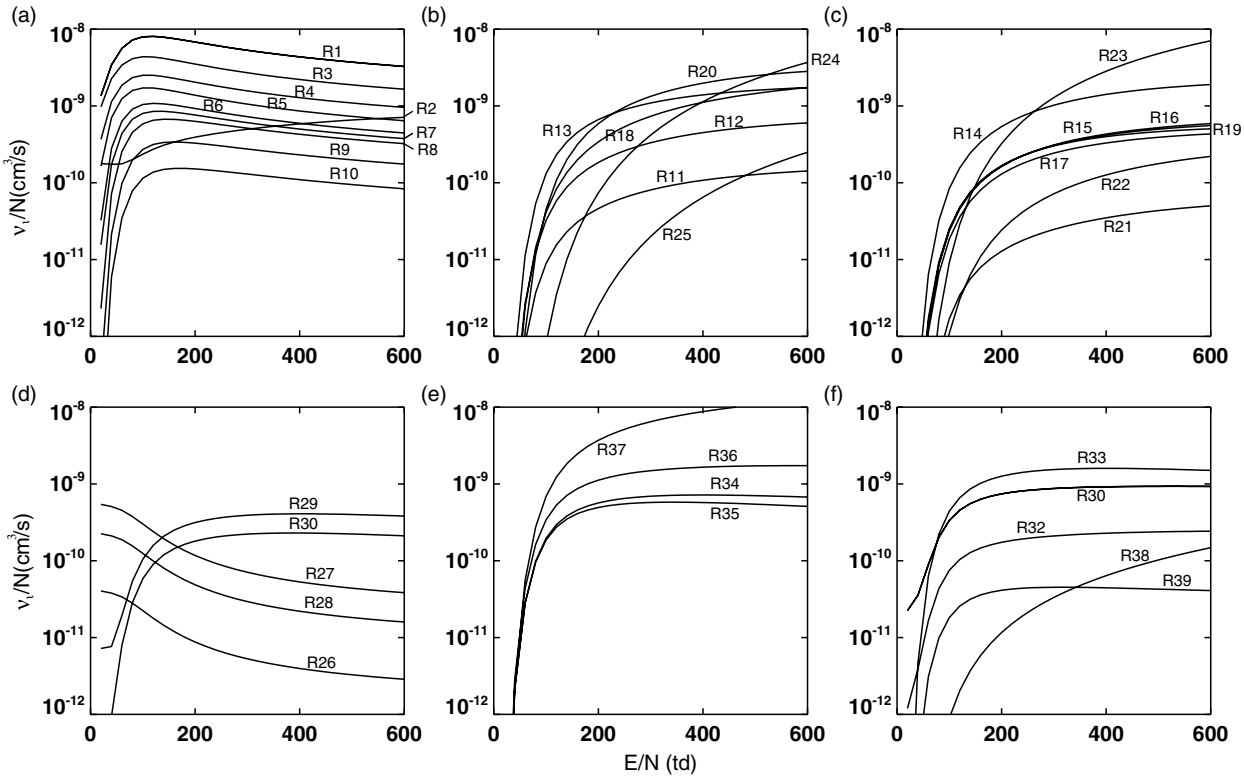

Figure 1. Reaction rates for the collisional processes of electrons with molecular nitrogen or molecular oxygen: (*a*) rates for N_2 rotational excitation and vibrational excitations; (*b*) and (*c*) rates for N_2 electronic excitations and ionizations; (*d*) rates for O_2 rotational excitation and vibrational excitations; (*e*) and (*f*) rates for O_2 electronic excitations, ionization, dissociations and two-body attachment where R# is the reaction listed in tables 1 and 2 for N_2 and O_2, respectively.

propagating sprite streamers [25, 35]. Due to the proximity, the regions near the streamer tip could have an E-field that is greater than the breakdown value. Therefore, the streamer tip is a region of high electron density, rapid-evolving electron-field driven processes and high-reacting rate chemical reactions [30]. In the breakdown region, the electron increasing rate from the ionization of N_2 and O_2 (see tables 1 and 2) is greater than the electron decreasing rate from the dissociative attachment (mainly $e + O_2 \rightarrow O^- + O$) and the three-body attachment ($e + O_2 + A \rightarrow A + O_2^-$; $A = N_2$ or O_2). The sprite streamer head is the brightest region of the radiative emissions and is the major source of visible photons. From the measured optical photons by the ISUAL filtered imager/SP, one can infer the total excited number for a specified emission band in sprites. Consequently, we can estimate the minimum energy needed to pump up a specified occupation number for an excited molecular band. After summing over all the required collisional energies for electrons to excite the observed optical emissions, the energy deposition in TLEs can be inferred. For halos or elves, a quasi-electrostatic field or an EMP from lightning discharges will produce similar effects on neutrals as those in the sprite streamer head and their energy deposition can also be obtained.

Here, we use the reduced E-field (E/N, where E is the magnitude of the E-field and N is the neutral density) to denote the strength of the electric field in the atmosphere. The units of reduced E-field are in Townsend ($1\,\mathrm{Td} = 10^{-21}\,\mathrm{V\,m^2}$).

3.1. Electrical field driven kinetic model

We use a time-dependent Boltzmann solver for partially ionized plasma (ELENDIF) [36], and calculate the rates of the collisional processes as a function of reduced E-field, $v_i(E_{\mathrm{reduced}})$. The kinetic model includes the rotational, vibrational and electronic excitation processes of electrons colliding with N_2 and O_2 as shown in tables 1 and 2. The cross section data used in ELENDIF is compiled by A V Phelps (http://jilawww.colorado.edu/~avp/collision_data/electronneutral/ELECTRON.TXT). The computed rates are shown in figure 1: figure 1(*a*) contains the rotational and vibrational excitations of electrons with N_2; figures 1(*b*) and (*c*) represent the electronic excitation of electrons with N_2; figure 1(*d*) shows the rotational and vibrational excitations of electrons with O_2; figures 1(*e*) and (*f*) present the electronic excitation of electrons with O_2 where the reaction pathways are listed in tables 1 and 2. One of the strongest emission bands for O_2 is the first negative band of molecular oxygen, ($1N\ O_2^+$; $b\,^4\Sigma_g^- \rightarrow a\,^4\Pi_u$). The branching ratio of the upper state ($b\,^4\Sigma_g^-$) of O_2^+ into the total ionization of O_2 is 0.24 [37] (p 138 and the references therein). The ionization process of O_2 (R38) is listed in table 2, and its reaction rate is shown in figure 1(*f*). The reaction rate of $1N\ O_2^+$ (R38 $\times$ 0.24) is substantially lower than that for $1PN_2$ (R13), $2PN_2$ (R20), LBH N_2 (R18) and $1NN_2^+$ (R25), see figure 1(*b*). Hence, $1N\ O_2^+$ emission is much weaker than that from molecular nitrogen.

The populating rates v_{1P} of the $N_2(B\,^3\Pi_g)$ for the $1PN_2$ band includes contributions from the excited states

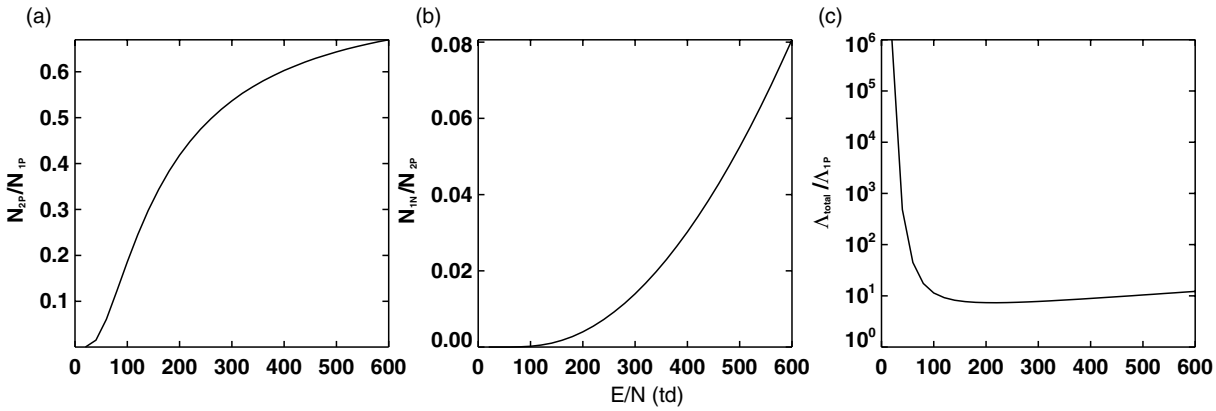

Figure 2. The population ratio of N_{2P} to N_{1P} (*a*) and N_{1N} to N_{2P} (*b*); (*c*) the ratio of the total energy deposition Λ_{total} to that in the $1PN_2$ band system Λ_{1P} as a function of reduced E-field, in units of Townsend.

Table 3. Excitation energy threshold, wavelength range, Einstein coefficients and quenching rates for the major emission band systems of nitrogen [13].

Emission band system	Transition	Excitation energy threshold (eV)	Wavelength (nm)	A_k (s^{-1})	k_{q,N_2}	k_{q,O_2}
$1PN_2$	$N_2(B\,^3\Pi_g) \rightarrow N_2(A\,^3\Sigma_u^+)$	~7.35	478–2531	1.7×10^5	1.60×10^{-11}	1.50×10^{-10}
$2PN_2$	$N_2(C\,^3\Pi_u) \rightarrow N_2(B\,^3\Pi_g)$	~11	268–546	2.0×10^7	1.12×10^{-11}	2.85×10^{-10}
LBH N_2	$N_2(a\,^1\Pi_g) \rightarrow N_2(X\,^1\Sigma_g^+)$	~8.55	100–260	1.8×10^4	2.20×10^{-11}	4.30×10^{-10}
$1NN_2^+$	$N_2^+(B\,^2\Sigma_u^+) \rightarrow N_2^+(X\,^2\Sigma_g^+)$	~18.8	286–587	1.6×10^7	4.53×10^{-10}	7.36×10^{-10}

of $N_2(W\,^3\Delta_u,\ B'\,^3\Sigma_u^-)$ through the intersystem collisional transfer (ICT). Another contribution to the $N_2(B\,^3\Pi_g)$ is the collisional deactivation of $N_2(a'\,^1\Sigma_u^-)$. The chemiluminescent emissions from $N_2(a'\,^1\Sigma_u^-)$ in the streamer tail of the sprite have been observed by high speed imager and have also been theoretically confirmed in the plasma chemical modelling of the sprite streamer [30] and the references therein. The total occupation number of a specified excited state from the electron impacts in the volume of a sprite is $N_i = \int \upsilon_i(E_{reduced})\,dt \approx \upsilon_i(\bar{E}_{reduced})\tau_{TLE}$, where $\bar{E}_{reduced}$ is time-averaged reduced E-field, and τ_{TLE} is the duration of the emission. Therefore, $N_{1P} \approx \upsilon_{1P}\tau_{TLE}$ can be expressed as $(\upsilon_{B\,^3\Pi_g} + \upsilon_{W\,^3\Delta_u} + \upsilon_{B'\,^3\Sigma_u^+} + \upsilon_{a'\,^1\Sigma_u^-})\tau_{TLE}$. The total occupation number N_{2P} of the $N_2(C\,^3\Pi_u)$ for $2PN_2$ is approximately $(\upsilon_{C\,^3\Pi_u} + \upsilon_{E\,^3\Sigma_g^+} + \upsilon_{a''\,^1\Sigma_g^+})\tau_{TLE}$, which is another contribution from $N_2(E\,^3\Sigma_g^+, a''\,^1\Sigma_g^+)$ through ICT [30]. In figures 2(*a*) and (*b*), the number ratios N_{2P}/N_{1P} and N_{1N}/N_{2P} are shown as functions of reduced E-field (20–600 Td). The $\bar{E}_{reduced}$ can be derived from the observed time-integrated photon emission ratios and it will be discussed in section 4.

We define the energy deposition rate as the reaction rate of a specified collisional process multiplied by the electron threshold energy, $\upsilon_i\varepsilon_i$; see figure 1 and tables 1 and 2. In all, we sum over the 39 collisional processes in tables 1 and 2 to obtain the total energy of electrons, $\Lambda_{total} = \sum_i \upsilon_i\varepsilon_i$, and to compute the ratio $\Lambda_{total}/\Lambda_{1P}$ between the total energy and the energy in $1PN_2$ emission $\Lambda_{1P} = \upsilon_{B\,^3\Pi_g}\varepsilon_{B\,^3\Pi_g} + \upsilon_{W\,^3\Delta_u}\varepsilon_{W\,^3\Delta_u} + \upsilon_{B'\,^3\Sigma_u^+}\varepsilon_{B'\,^3\Sigma_u^+} + \upsilon_{a'\,^1\Sigma_u^-}\varepsilon_{a'\,^1\Sigma_u^-}$, as shown in figure 2(*c*). The ratio $\Lambda_{total}/\Lambda_{1P}$ can be used to compute the total energy deposition if Λ_{1P} is known from TLE observation and the reduced E-field can be derived from observation or from previous theoretical modelling [26]. The reason why we choose to compute $1PN_2$ energy deposition but not others is that all the TLEs studied here were recorded through the $1PN_2$ filter as stated in the Introduction.

3.2. Theoretical spectra of TLEs

To correctly restore the band emissions from ISUAL data, we need to estimate the percentage of photons which passed through the filtered Imager/SP. The first step to recover the information is to simulate the TLE spectra. We calculate the theoretical wavelength of the emission lines for different upper and lower states of a specified band in molecular nitrogen. In Born–Oppenheimer approximation, the energy of the states for a diatomic molecule like nitrogen can be decomposed into the electronic, vibrational and rotational term energies, respectively [38]. As an example, for $1PN_2$ we consider the upper state $N_2(B\,^3\Pi_g)$ and the lower state $N_2(A\,^3\Sigma_u^+)$; States for other emission bands are listed in table 3. The specified energy level $E_{e,v,J}$ (cm^{-1}) of the upper state or the lower state of a given emission band in molecular nitrogen can be expressed as a sum of the electronic term energy T_e (cm^{-1}), the vibrational term energy $G(v)$ and the rotational term energy $F_v(J)$,

$$E_{e,v,J} = T_e + G(v) + F_v(J), \tag{1}$$

where $G(v)$ and $F_v(J)$, in units of cm^{-1}, can be fitted using the Klein–Dunham polynomial expansions for the specified vibrational quantum number v and the specified rotational quantum number J of the energy level. The formulae for calculating the vibrational and rotational term energies, $G(v)$

and $F_v(J)$, can be truncated to four and two terms, respectively, and are approximately equal to

$$G(v) \approx \omega_e(v+\tfrac{1}{2}) - \omega_e\chi_e(v+\tfrac{1}{2})^2 + \omega_e y_e(v+\tfrac{1}{2})^3 + \omega_e z_e(v+\tfrac{1}{2})^4, \quad (2)$$

$$F_v(J) \approx [B_e - \alpha_e(v+\tfrac{1}{2})]J(J+1) - [D_e + \beta_e(v+\tfrac{1}{2})]J^2(J+1)^2. \quad (3)$$

Here the related parameters in units of cm^{-1} (T_e, ω_e, χ_e, y_e, z_e, α_e, β_e, B_e and D_e) for $1PN_2$, $2PN_2$, $1NN_2^+$ are compiled in [39] (table 1) and for N_2 LBH in NIST Chemistry WebBook (http://webbook.nist.gov). For the vibrational term energy, we consider the vibrational numbers $v' = 0$–10, $v' = 0$–4, $v' = 0$–2 for the upper electronic states of $1PN_2$, $2PN_2$ and $1NN_2^+$. The reason for selecting these vibrational numbers for each band emission is to compute only those that produce significant radiation in the ISUAL detectable range of 180–800 nm. For N_2 LBH, we select $v' = 0$–11 to cover the major emissions between 180 and 260 nm. Below 180 nm, the absorption due to the Schumann–Runge continuum and the Schumann–Runge band in molecular oxygen becomes very severe. Therefore, nearly no emission below 180 nm can be detected by the ISUAL instrument; the same reason is also applicable when calculating the atmospheric transmittance [13, 27].

To compute the fine nitrogen spectral lines, we based our work on [39] to minimize the errors. We dropped the second term because D_e and β_e are six orders of magnitude lower than B_e, as shown in [39] (table 1). Therefore, equation (3) becomes $F_v(J) \approx [B_e - \alpha_e(v+\frac{1}{2})]J(J+1)$. The three sub-levels for triple states ($A\,^3\Sigma_u^+$, $B\,^3\Pi_g$, $C\,^3\Pi_u$) and 2 sub-levels for doublet states ($X\,^2\Sigma_g^+$, $B\,^2\Sigma_u^+$) from the spin degeneracy can be replaced with a single level because the energy gap between the sub-level is significantly smaller than that in the radiative transition. The selection rule is $\Delta J = J' - J'' = 0$, or ± 1, where J' and J'' are the rotational quantum numbers in the upper and the lower electronic states of the specified band for molecular nitrogen. The maximum value of J' is 40 in our calculation. The wavelength λ is determined from the energy difference of the upper electronic state E_u and the lower electronic state E_l for a given band emission,

$$\lambda = \frac{1}{E_u - E_l}, \quad (4)$$

where E_u and E_l are defined in equation (1) in units of wavenumber (cm^{-1}).

The intensity of a given emission line depends on the transition probability between the upper state and the lower state (the branch ratio), and the number densities of the vibrational and rotational levels of the upper electronic state in a specified band. For direct electron impact in discharge phenomena, the pumping density of a specified vibrational level v' of the upper state u is proportional to the Franck–Condon factor $q_{0v'}^{Xu}$, which is the transition probability from the 0th vibrational level of the ground state X to the v'th vibrational level of the upper electronic state u of the specified band system. We define the vibrational relaxation time as the time for the redistribution of the vibrational levels in the upper electronic state of the specified band emission. If the vibrational relaxation time is longer than the time scale considered, the vibrational levels will reach a quasi-equilibrium. Then, the number density distribution $N_{v'}^u$ for the v'th vibrational level of the u upper electronic state in a specified band system can be expressed as

$$\frac{N_{v'}^u}{N^*} \approx \frac{\exp\left[-\dfrac{hc}{kT_{v'}}G(v')\right]}{\sum_{v'}\exp\left[-\dfrac{hc}{kT_{v'}}G(v')\right]}, \quad (5)$$

where h is the Planck constant (6.63×10^{-34} J s), c is the light speed in vacuum (10^{10} cm s^{-1}) and k is the Boltzmann constant (1.38×10^{-23} J K^{-1}); N^* denotes the total excitation number density for the specified band system. The distribution of the vibrational levels can be described by the Boltzmann temperature $T_{v'}$, where $T_{v'}$ which is close to the kinetic temperature of thermal electrons if the vibrational-electronic energy exchange is very efficient [40]. From the relative number densities of the vibrational levels in the observed sprite spectra, the Boltzmann temperature $T_{v'}$ is found to be close to 1 eV for $N_2(B\,^3\Pi_g)$ in the $1PN_2$ band system and is 10–25 eV for $N_2^+(A\,^2\Sigma_u^+)$ in the Meinel N_2^+ band system [41, 42].

However, the time scale of the vibrational relaxation for molecular nitrogen at higher temperature ($T_{v'} > 1$ eV) also satisfies the empirical law $p\tau_{v'} \sim 10^{-8}$ atm s; where p is the gas pressure in units of normal atmospheric pressure (atm) and $\tau_{v'}$ is the vibrational relaxtion time in units of s [43]. If the vibrational levels can be redistributed, the time scale of the vibrational redistribution must be shorter than the lifetime of the emission band. The typical lifetime of the emission band is $\sim 6\,\mu$s for $1PN_2$; since $\tau_k = 1/A_k$ and for the value of A_k for $1PN_2$ listed in table 3. Above the 45 km altitude, $p < 1.4 \times 10^{-3}$ atm [44] and $\tau_{v'} > 7\,\mu$s. The vibrational relaxation time is longer than the lifetime of the $1PN_2$ band. The altitudes of optical emissions in sprites, elves and halos are higher than 45 km. Hence, in our spectra calculation, the distribution of the vibrational levels can be approximated as $N_{v'}^u/N^* \approx q_{0v'}^{Xu}$ which is a result of direct electron impact.

For the relative distribution of the rotational levels in molecular nitrogen, the energy separation between adjacent rotational levels is small in comparison with the translational kinetic energy. The energy exchange rates between the transitional and rotational states are high; therefore the equilibrium temperature of the rotational distribution is very close to the molecular translational temperature [40]. The distribution of the rotational level with rotational number J at molecular rotational temperature T_R in units of absolute temperature (K) can be expressed as

$$\frac{N_{v'J'}^u}{N_{v'}^u} \approx \frac{(2J'+1)\exp\left[-\dfrac{hc}{kT_R}F_{v'}(J')\right]}{\sum_{J'}(2J'+1)\exp\left[-\dfrac{hc}{kT_R}F_{v'}(J')\right]}, \quad (6)$$

where the rotational term energy $F_v(J')$ is defined in equation (3), and T_R is the molecular rotational temperature,

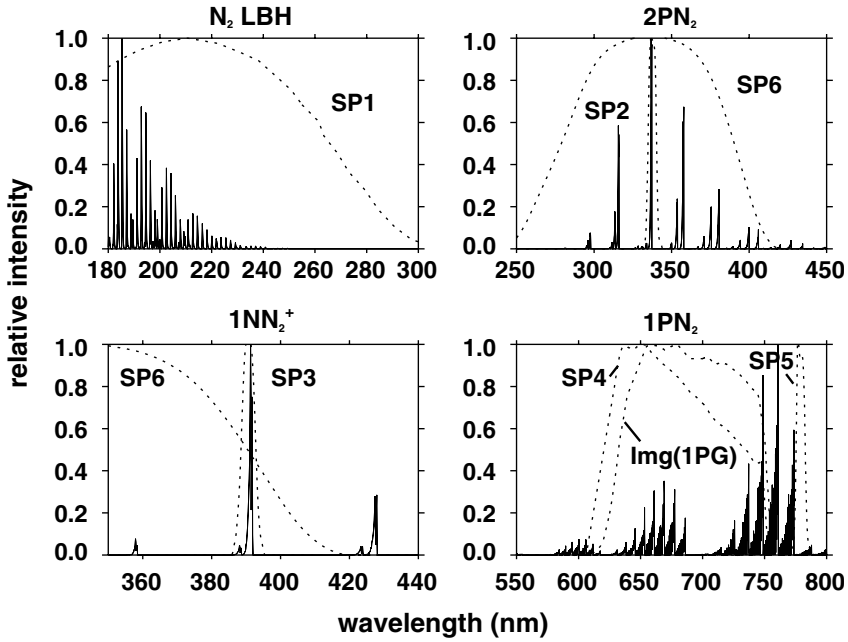

Figure 3. Theoretical spectra of the major molecular nitrogen band systems, $1PN_2$, $2PN_2$, N_2 LBH and $1NN_2^+$, in TLEs. The relative intensities of the vibrational-rotational lines are computed at the rotational temperature $T_R = 210$ K. The $1PN_2$ imager filter and the passing bands of the ISUAL SP channels are plotted with dashed lines.

which is also the molecular translation temperature. The molecular translation temperature is between 190 and 230 K at 70–90 km altitudes. To compute a typical TLE spectrum, we adopt the mid-value, 210 K, as the rotational temperature.

The intensity of the emission from the v'th vibrational level of the upper electronic state u to the v''th vibrational level of the lower electronic state l in a specified molecular band system can be expressed as $N^{\mathrm{u}}_{v'} A^{\mathrm{ul}}_{v'v''}$; the adopted values of transition probability $A^{\mathrm{ul}}_{v'v''}$ between the v'th vibrational level of the upper state u and the v''th vibrational level of the lower state l and the Franck–Condon factors are listed in [45]. To compute the vibrational-rotational spectrum that follows the selection rule $\Delta J = 0, \pm 1$, we consider the P branch $\Delta J = +1$, Q branch $\Delta J = 0$ and the R branch $\Delta J = -1$ for the band emission in molecular nitrogen.

The calculated sprite spectra in N_2 LBH, $1PN_2$, $2PN_2$ and $1NN_2^+$ are shown in figure 3. For a specified emission band, the intensity of the emission line is in a relative scale. The passing bands of the ISUAL imager and SP are also overlaid with the calculated band emissions for easy reference.

3.3. The percentage of total excited number of emission bands into imager/SP data

The percentage contribution of emission bands to the ISUAL imager and the SP readings can be used to convert the ISUAL detected photons to the total excited number of the upper state in a specified band of molecular nitrogen. Due to the quenching effect, only part of the excited molecular nitrogen emits photons. In addition, photons would be absorbed and scattered before they enter into ISUAL detectors. The major band emissions of molecular nitrogen, see figure 3, have different intensities at various wavelengths, and Imager/SP also have different sensitivities at different wavelengths. Hence, the weighting effect at various wavelengths also needs to be considered. Therefore, the molecular band percentages, $B_k(h, L)$, are defined by

$$B_k(h, L) = \frac{\sum_\lambda I_k(\lambda) T(\lambda, h, L) R(\lambda) q_k(h) \Delta\lambda}{\sum_\lambda I_k(\lambda) \Delta\lambda}, \qquad (7)$$

where $I_k(\lambda)$ is the band emission from $1PN_2$, $2PN_2$, N_2 LBH or $1NN_2^+$, and $T(\lambda, h, L)$ is the atmospheric transmittance, which is a function of wavelength λ, the assumed altitude h of TLE and the distance L between the TLE and the satellite. The quenching factor $q_k(h)$ will be defined shortly and $R(\lambda)$ is the imager/SP relative response function. The relative response function for the imager and SP4 equipped with the $1PN_2$ filter was set to unity at 690 nm; others are at 210.8 nm, 337 nm, 391.4 nm and 326 nm for SP1, SP2, SP3 and SP6, respectively. The absolute brightness of the filtered imager and all the SP channels have been pre-flight calibrated in units of Rayleigh and in photon intensity (photons $\mathrm{cm}^{-2}\,\mathrm{s}^{-1}$).

Quenching means that the metastable molecules in the excited state collide with low-energy molecules and lose the excitation energy without radiating photons [37, p 119]. The quenching factor at an altitude h is defined as

$$q_k(h) = \left\{ 1 + \frac{k_{q,\mathrm{N}_2} N_{\mathrm{N}_2}(h) + k_{q,\mathrm{O}_2} N_{\mathrm{O}_2}(h)}{A_k} \right\}^{-1}, \qquad (8)$$

where the quenching ratios are k_{q,N_2} for nitrogen and k_{q,O_2} for oxygen. For the upper states of the molecular band systems, the values for k_{q,N_2}, k_{q,O_2} and the radiative transition probability A_k are listed in table 3. The quenching factor sensitively depends on the density of nitrogen and oxygen and hence is a function of altitude h. In our calculation, we assume that the sprite is at 70 km altitude. Similarly, halos and elves are assumed at the altitudes of 80 km and 90 km, respectively.

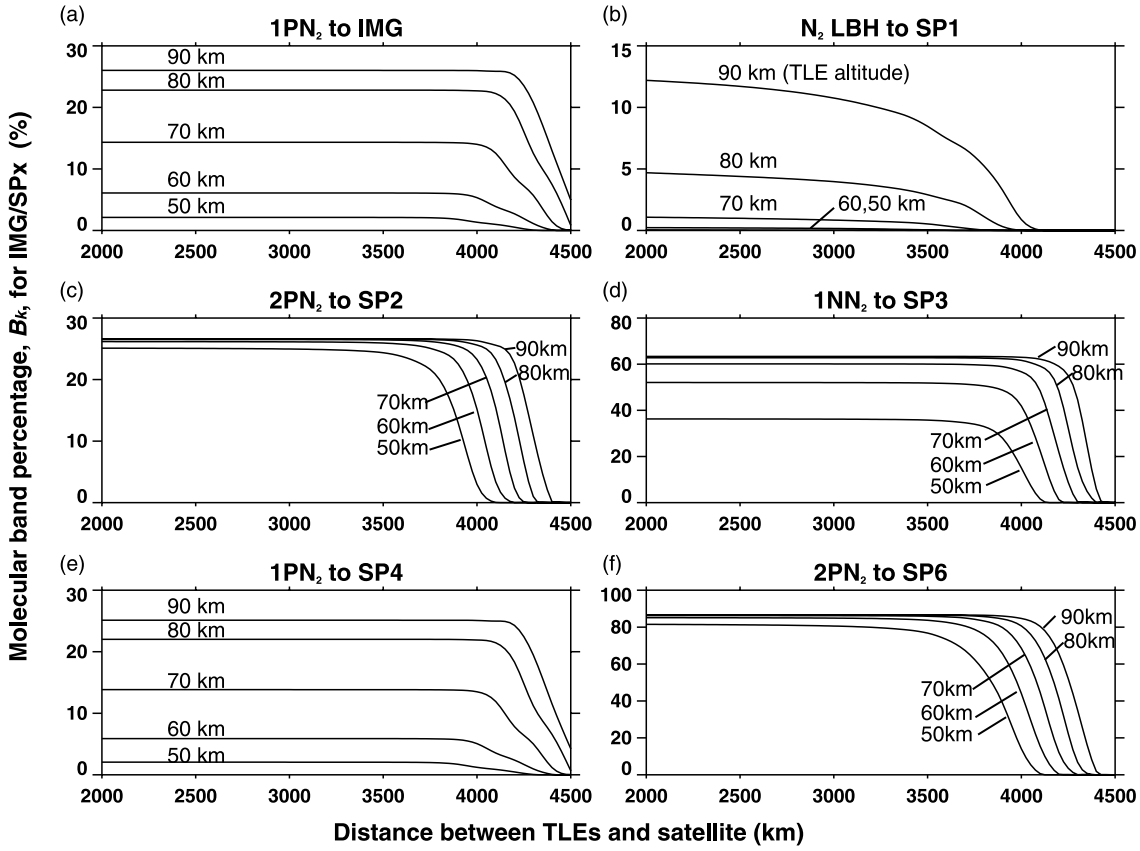

Figure 4. The percentage (%) of the molecular nitrogen band ($1PN_2$, $2PN_2$, N_2 LBH and $1NN_2^+$) to the $1PN_2$-filtered imager and SPx at event distances of 2000–4500 km. Only the TLE emissions originated at altitudes of 50, 60, 70, 80 and 90 km were considered.

The atmospheric transmittance along the line of sight will affect the percentage of band emission, B_k, and, can be calculated using Lamber's law, $T(\lambda, h, L) = \exp[-\sum_x \sigma_x(\lambda) D_x(h, L)]$, where $\sigma_x(\lambda)$ is the absorption cross section in units of cm^2 for the major atmospheric species: O_2 absorption, O_3 absorption and molecular Rayleigh scattering (N_2, O_2). The absorption cross section of N_2 is very small between 185 and 800 nm, and its effect on the transmittance is negligible [46, pp 22–4]. The absorption cross sections data for molecular oxygen, ozone and molecular Rayleigh scattering were compiled in [13]. The column density in units of cm^{-2}, $D_x(h, L)$, is calculated by integrating density of N_2, O_2, O_3 along the path from FS-2 to the assumed altitude h of TLE, $D_x(h_{TLE}, L) = \int_{FS\text{-}2}^{h_{TLE}} n_x(s)\,ds$. The total length of the path between FS-2 and the TLE is L. The geometry is shown in figure 6(*d*). The density of N_2 and O_2 is computed using the MSIS model [47]. The night-time ozone density profile between 18 and 100 km altitude was from the MIPAS measurement (Michelson interferometer for passive atmospheric sounding) [48]. The ozone below 100 km accounts for the majority of ozone absorption in our calculated atmospheric extinction.

Figure 4 shows the percentage of the excited number B_k, equation (7), for the $1PN_2$, $2PN_2$, N_2 LBH, $1NN_2^+$ bands that contribute to the imager/SP bandpass reading. For example, in figure 4(*a*), B_k of the $1PN_2$ band to the $1PN_2$-filtered Imager is ∼26% if the altitude of TLE optical emission is ∼90 km, and the distance between the TLE and FS-2 is 3500 km. For a lower altitude (80, 70, 60 and 50 km shown in figure 4), the band percentage is clearly lower than that for 90 km. The band percentage, B_k, is lower because the denser low-energy molecules could absorb the radiative energy from the excited nitrogen and later release the energy through quenching.

4. Results

To compute the energy deposition in the upper atmosphere by TLEs, we adopt the following procedures: first, we calculate the SP measured time-integrated photon intensity (photons cm^{-2}). Second, we derive the distance r between the TLE and the FS-2 satellite. From the satellite orbital information, we can obtain the nadir angle of the ISUAL viewing direction. Relative to the centre of FOV, the viewing angle of each imager pixel can be deduced since each pixel spans a FOV of ∼0.04°. As an example, the observational geometry for an ISUAL recorded halo is shown in figure 6(*d*). Since the FS-2 altitude is 891 km and the halo altitude is assumed to be ∼80 km, from the centre of the halo in the ISUAL image frame we can calculate the nadir angle of the projecting ray out of the centre pixel of the halo. The projecting ray out of this pixel is indicated by the solid line, which links the satellite and the halo as shown in figure 6(*d*). For a triangle with three vertices (FS-2, the centre of the halo and the Earth centre), the angle α and two sides (FS-2 to the Earth centre and halo to the Earth centre) can be obtained. The length of the third side gives the distances between FS-2 and halos. The

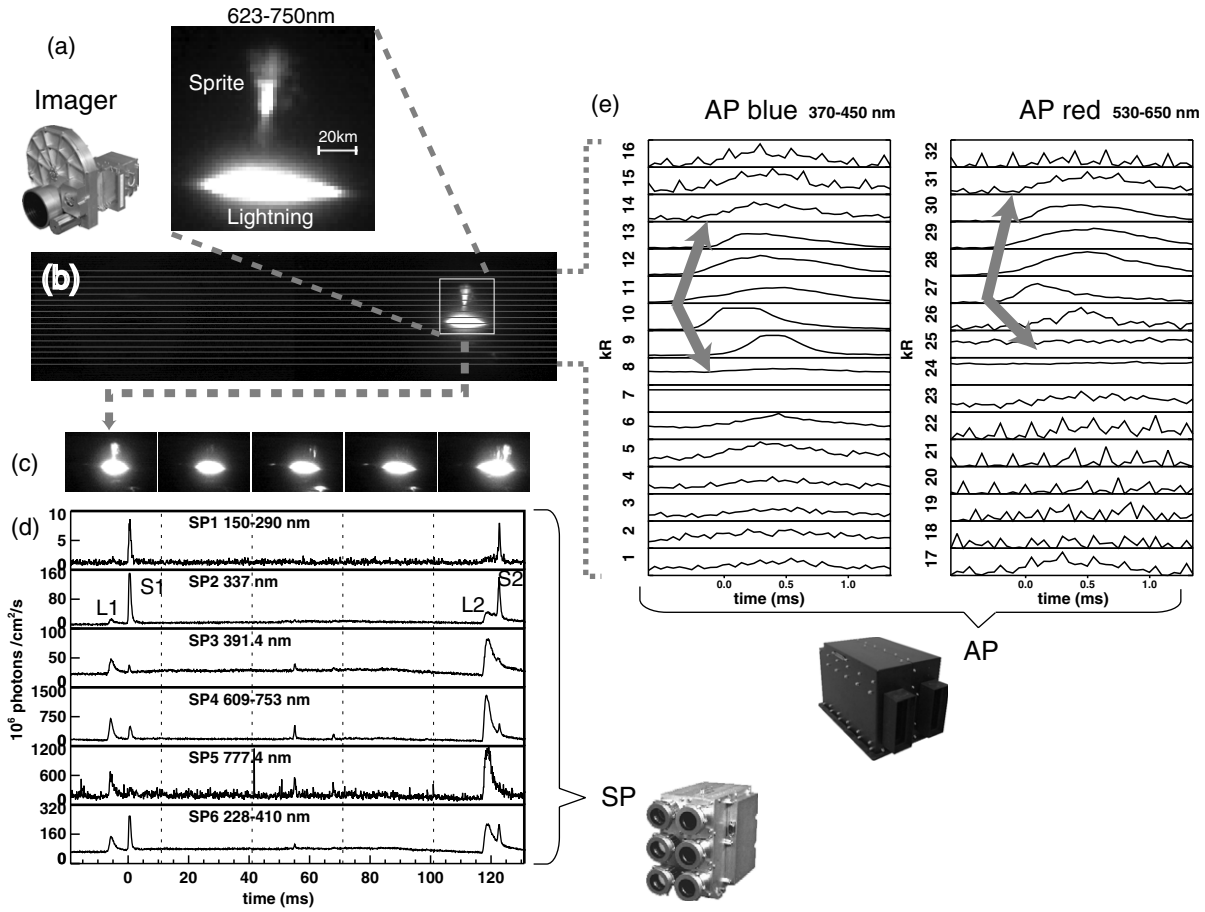

Figure 5. (*a*) ISUAL imager and the cropped image frame of the sprite recorded on 18 July 2004 21:30:15.316 UTC, (*b*) the original image frame of this sprite; the white lines represent the FOV of the AP channels, (*c*) image sequence of the sprites with 29 ms integration time and 1 ms image readout dead time, (*d*) photometric traces for the sprites where S1/S2 and L1/L2 denote the peaks from the sprites and their parent lightning and (*e*) AP signal traces from the blue and red modules. The AP signal traces indicate that the sprite initiated at AP channel #11/#27 and propagated upwards and downwards almost simultaneously [26].

length has two possible solutions, behind the limb or in front of the limb, but the image data can be used to resolve them without ambiguity.

Assuming isotropic emissions and multiplying the SP time-integrated photon intensity by $4\pi r^2$, we obtain the number of photons from a specified SP band for a TLE. Third, we convert the SP measurements into the total excited numbers for the $1PN_2$, $2PN_2$, N_2 LBH, $1NN_2^+$ bands using the band percentage, B_k. Fourth, we multiply the excited number in each band by its threshold energy as listed in table 1. Finally, we sum the energy deposition contribution from all the molecular nitrogen emission bands ($1PN_2$, $2PN_2$, N_2 LBH, $1NN_2^+$) to obtain the TLE energy associated with radiative emissions. However, the estimated energy deposition is based on the major emissions in the TLEs, which is definitely only a fraction of the total energy deposition in molecular nitrogen from the TLE-inducing quasi-static E-field or electromagnetic field. The excited number in the rotational levels, the vibrational levels and other electronic bands that do not produce optical emissions should also be considered. Their contributions to the energy deposition can be properly accounted for through the converting factor $\Lambda_{\text{total}}/\Lambda_{1P}$ as defined in section 3.1.

4.1. Sprites

Figure 5 shows the ISUAL imager, SP and AP data for a sprite that occurred on 18 July 2004 21:30:15.316 UT. The $1PN_2$-filtered imager measured the sprite brightness in units of Rayleigh with a time average of 29 ms per frame. One Rayleigh is defined as the magnitude of the column-integrated emission along the line of sight and is equal to 10^6 photons cm^{-2}-column s^{-1}. The temporally and spatially averaged brightness from the $1PN_2$-filtered imager for this sprite is 3.2 MR, and the brightness for the brightest pixel of $\sim 2 \times 2$ km in this sprite is 13.5 MR. As shown in figure 5(*c*), a sprite occurred and concluded in the first frame, and a second sprite appeared in the fifth frame. Figure 5(*c*) is a typical image sequence for the so-called dancing sprites. Figure 5(*d*), the higher time resolution SP data, indicates that the leading peak (labelled L1 and L2) is from the lightning emissions while the second peak (labelled S1 and S2) is from the sprite emissions. The SP traces indicate that these sprites were clearly separated and delayed from their parent lightning. At the estimated distance of $\sim$3000 km between these sprites and the FS-2 satellite, each AP channel covered a vertical height of 12 km. The altitude-resolved signal traces from AP blue and red modules are displayed in figure 5(*e*). From the AP altitude and time

Table 4. The derived energy deposition of selective TLEs from ISUAL observations.

TLE	Total excited number of molecular band				Energy deposition (MJ)				$\frac{\Lambda_{total}}{\Lambda_{1P}}$	Λ_{total} (MJ)
	$1PN_2$	$2PN_2$	LBH	$1NN_2^+$	$1PN_2$	$2PN_2$	LBH	$1NN_2^+$		
Sprite S1	2.7×10^{24}	6.0×10^{23}	9.3×10^{23}	1.2×10^{22}	3.18	1.06	1.27	0.04	10	31.8
Sprite S2	1.5×10^{24}	3.6×10^{23}	6.1×10^{23}	1.2×10^{22}	1.76	0.63	0.83	0.04	10	17.6
Halo	4.5×10^{23}	4.4×10^{22}	N/A	1.5×10^{21}	0.53	0.08	N/A	0.005	10	5.3
Elve	1.5×10^{24}	2.0×10^{23}	N/A	4.8×10^{21}	1.76	0.35	N/A	0.014	10	17.6
Gigantic jet	7.9×10^{23}	1.7×10^{23}	5.1×10^{22}	1.6×10^{22}	0.93	0.3	0.07	0.05	10	9.3

resolving data, the upward and downward propagation speed in these sprites is estimated to be $\sim 6 \pm 3 \times 10^7\,\mathrm{m\,s^{-1}}$. This propagation velocity is similar to that for the sprite streamers observed in ground observations [49, 50].

After the lightning contamination in the SP signal was subtracted through an exponential curve-fitting estimation of the lightning contribution, the time-integrated photon intensity for SP1, SP2, SP3, SP4 and SP6 are 6.6×10^3 photon $\mathrm{cm^{-2}}$, 1.4×10^5 photon $\mathrm{cm^{-2}}$, 6.4×10^3 photon $\mathrm{cm^{-2}}$, 3.3×10^5 photon $\mathrm{cm^{-2}}$ and 1.8×10^5 photon $\mathrm{cm^{-2}}$, respectively. The percentage contribution of imager/SP measured photons to the total excited number of molecular nitrogen bands ($1PN_2$, $2PN_2$, LBH and $1NN_2^+$) is the molecular band percentage (B_k). The B_k is shown in figure 4 and is defined in equation (7); note that the B_k has been corrected for the quenching effect and the atmospheric transmittance at different altitudes of emissions. Although the altitudes of sprite emissions range from 40 to 90 km, we use the middle value of B_k at 70 km altitude for sprites to reduce the possible errors caused by the spread of emission altitude. For the sprite event shown in figure 5, the event distance is ~3000 km. The band percentage at 70 km altitude are 0.8% of N_2 LBH into SP1, 26.5% of $2PN_2$ into SP2, 60.1% of $1NN_2^+$ into SP3, 13.8% of $1PN_2$ into SP4 and 86.2% of $2PN_2$ to SP6 (see figure 4).

The measured time-integrated photon intensity from SP4 ($1PN_2$) is 3.3×10^5 photons $\mathrm{cm^{-2}}$. Assuming isotropic emissions, the total detected photon number at the sprite is $3.3 \times 10^5 \times 4\pi \times (3 \times 10^8)^2 = 3.7 \times 10^{23}$ photons. The total excited number of the $1PN_2$ band as derived from SP4 is $3.7 \times 10^{23}/13.8\% = 2.7 \times 10^{24}$. In a similar manner, the excited numbers for LBH, $2PN_2$ and $1NN_2^+$ bands can be derived from SP1, SP2 and SP3 readings and are $\sim 9.3 \times 10^{23}$, 6.0×10^{23} and 1.2×10^{22}. Here, we derive the photon number of $2PN_2$ from SP2 but not from SP6 for two reasons: the passing band of the broadband SP6 covers both the $2PN_2$ and the $1NN_2^+$ bands; the photon sensitivity of SP6 is angle-dependent as it has a different photocathode size as compared with the other SP PMTs. The relative response function of SP6 is flat when the event angle is less than 3° from the normal direction, but drops sharply when the event's slant angle exceeds 3°. After multiplying the excited number by the threshold electron energy (7.35 eV for $1PN_2$, see table 4), the total energy deposition of $1PN_2$ is computed to be 3.18 MJ; see table 4 for other TLEs.

The excited number ratios of $2PN_2$ to $1PN_2$ are $N_{2P}/N_{1P} = 6.0 \times 10^{23}/2.7 \times 10^{24} = 0.22$ and 0.24 for sprites S1 and S2, while N_{1N}/N_{2P} are 0.02 and 0.03 for the same two sprites listed in table 4. Based on the number ratio of N_{2P}/N_{1P} in figure 2(*a*) and the method discussed in section 3.1, the time-averaged reduced E-field $\bar{E}_{reduced}$ are derived to be ~112 and ~118 Td for sprites S1 and S2. These reduced E-fields are very close to the modelled breakdown E-field, $E_k \sim 120$ Td, which is calculated using ELENDIF and at the E-field strength that results in equality between the dissociative attachment and the ionization rates. However, using the number ratio of N_{1N}/N_{2P} in figure 2(*b*), the derived time-averaged reduced E-field, $\bar{E}_{reduced}$ would be ~341 and ~399 Td for the same two sprites. The reduced E-field derived from the time-integrated emission is consistent with that computed from the peak emission as reported in [26] (243–443 Td). Obviously, the difference in the derived $\bar{E}_{reduced}$ based on N_{2P}/N_{1P} and N_{1N}/N_{2P} were caused by the spatial averaging since in the streamer head region the reduced E-field was reported to be as high as $5E_k$ [27]. From figure 2(*c*), the ratio of the total energy deposition to that in the $1PN_2$ band $\Lambda_{total}/\Lambda_{1P}$ is ~10 between 95 and 600 Td. Since the energy deposition is 3.2 MJ and 1.76 MJ for $1PN_2$ band emission in sprites S1 and S2, the corresponding total energy deposition is ~32 MJ and 17.6 MJ, respectively; see also table 4.

We analysed 155 ISUAL recorded sprites that have clean or lightning emission subtractable SP reading. The average brightness of the $1PN_2$-filtered ISUAL sprites is found to be 1.5 ± 1.1 MR and the maximum is 27.4 MR. The average deposited energy in $1PN_2$ for the analysed events is 2.2 MJ. Following the calculation described above and $\Lambda_{total}/\Lambda_{1P} = 10$, the average deposited energy in the upper atmosphere is 22 MJ per sprite. The volume occupied by a sprite is $\sim 10 \times 10 \times 10\,\mathrm{km^3}$, which is equal to $1 \times 10^{12}\,\mathrm{m^3}$. The average energy density is $2.2 \times 10^{-5}\,\mathrm{J\,m^{-3}}$ in a sprite. The specified heat of air at constant pressure is $1.005\,\mathrm{J\,g^{-1}\,K^{-1}}$. The air density is $1.5 \times 10^{21}\,\mathrm{m^{-3}}$ at an altitude of 70 km, and average air mass is 28.8 amu. The mass of air in a volume of $1\,\mathrm{m^3}$ is 0.072 g. Therefore, on average the air temperature will be heated up by 3×10^{-4} K inside the luminous region of a sprite. Therefore, the air temperature increment due to sprites is very low.

4.2. Halos

For the ISUAL halos that occurred in front of the limb, the delay time between the parent lightning and the halo emission is too short (<0.1 ms) to make the halo emission extraction possible. Only halos that occurred behind the limb can be properly analysed. Figure 6 shows such an ISUAL recorded halo on 31 July 2006 06:26:29.850 UTC. We assumed that the halo's altitude is 80 km [17]. The distance between this

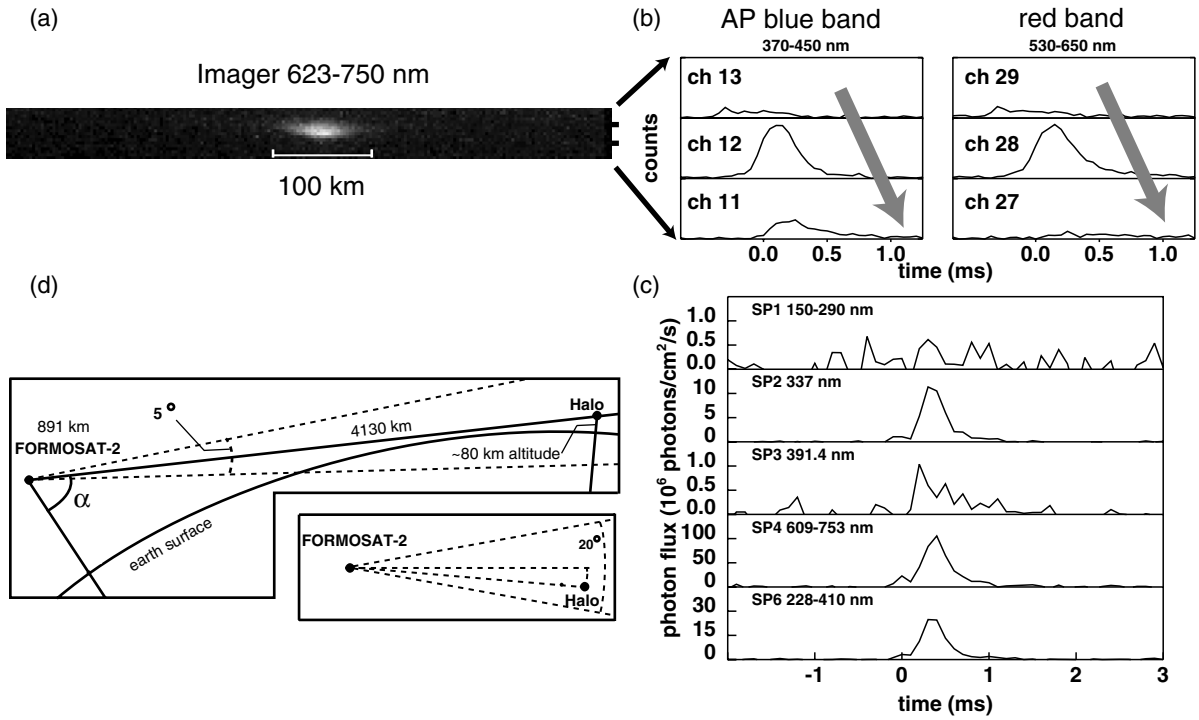

Figure 6. ISUAL recorded halo on 31 July 2006 06:26:29.850 UTC: (*a*) the imager data for this pancake-shaped halo, (*b*) AP data indicate that this event exhibited an apparent downward propagating motion, (*c*) the SP photometric traces and (*d*) the observational geometry for this halo with an estimated event distance of 4130 km.

halo and the FS-2 satellite is 4130 km. At this event distance, the diameter of this halo is ∼77 km (figure 6(*a*)). The spatially averaged brightness is 206 kR, and the maximum brightness for a pixel (covering a ∼2 km × 2 km region in this halo) is 553 kR.

Figure 6(*c*) shows that the time-integrated photon intensities in SP2, SP3 and SP4 are 4.1×10^3, 4.0×10^2 and 4.3×10^4 photons cm^{-2}. For SP1, the signal-to-noise ratio for the halo emission is too low, and the estimated time-integrated photon intensity for SP1 is less than 1.5×10^2 photons cm^{-2}. The band contribution of N_2 LBH to SP1 with a distance of 4130 km is less than 0.01%, and most of LBH emission is expected to be absorbed by the atmosphere. The deduced energy deposition in $1PN_2$ is 0.81 MJ. The reduced E-fields are ∼400 Td as derived from the N_{1N}/N_{2P} ratio. Following the same calculation prescribed in section 4.1, the ratio of total energy Λ_{total} to $1PN_2$ energy Λ_{1P} is 10. Therefore, the estimated total energy deposition is 5.3 MJ (table 4).

From the analysis of 55 ISUAL halo events, the average brightness based on $1PN_2$-filtered imager data is 0.3 ± 0.1 MR and the maximum brightness is 0.75 MR. The average energy deposition in the $1PN_2$ band emission of halos is 1.4 MJ, and the total deposited energy in the upper atmosphere is 14 MJ. The volume of the halo is $\pi \times 40 \times 40 \times 10$ km^3, which is equal to 5×10^{19} m^3. The average energy density increase due to a halo is 7.1×10^{-13} J m^{-3}, which is substantially lower than that in a sprite.

4.3. Elves

Along the same lines, the analysis of elves was feasible only for those occurring behind the limb when emissions from their parent lightning were blocked by the solid Earth. Figure 7 exhibits such an event which was recorded on 7 August 2004 1801:22 UT. From the imager data in figure 7(*a*), the diameter of elves is deduced to be ∼420 km. The maximum brightness in the optical emission is 646 kR and the spatially averaged brightness is 332 kR (see also the discussions in [13, 14]). The altitude of the elves is assumed to be 87 km and it coincided with the airglow layer. As seen in figures 7(*b*) and (*c*), the ISUAL SP and AP data are clean and without the lightning pollution. The calculated excited numbers of the major nitrogen emission bands and the band contribution to the energy deposition are listed in table 2. The reduced E-fields are ∼342 Td as derived from the ratio N_{1N}/N_{2P}. Hence, the ratio of total energy Λ_{total} to $1PN_2$ energy Λ_{1P} is ∼10, the same as those for the sprites and halos.

In this work, 1205 ISUAL recorded elves were analysed. The average brightness based on the $1PN_2$-filtered data was found to be 0.17 ± 0.08 MR and the maximum brightness is 0.71 MR. On averages, the $1PN_2$ band emission in an elve deposits 1.9 MJ of energy to the lower ionosphere. Following the method prescribed before, the energy transported by an elve to the upper atmosphere from all the nitrogen band emissions was 19 MJ. The volume occupied by an elve is $\pi \times 200 \times 200 \times 10$ km^3, which is equal to 1.3×10^{21} m^3. Hence an elve produces an energy density increase of 4×10^{-14} J m^{-3} in the region of the elve, which is also much lower than that of a sprite.

4.4. Gigantic jet

Figure 8 shows the image sequence of an ISUAL recorded GJ (28 May 2007 06:34:08.666 UT). The bright emission

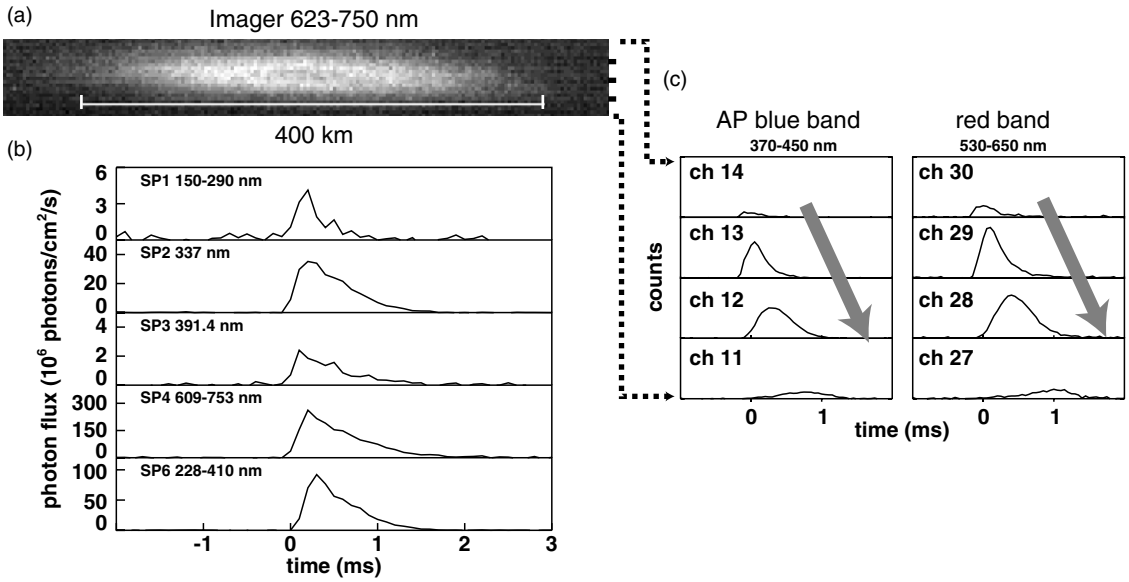

Figure 7. ISUAL elve on 7 August 2004 18:01:22.742 UTC; this doughnut-shaped event as seen in the imager (*a*), the SP (*b*) and the AP (*c*).

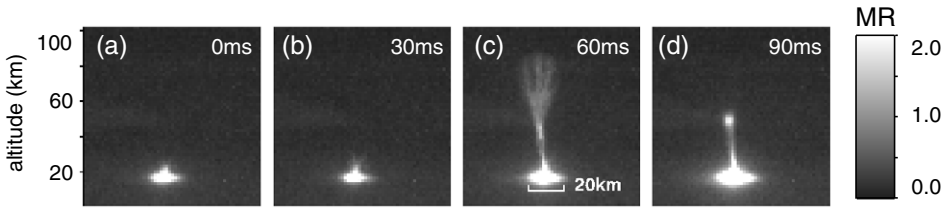

Figure 8. Time sequence of an ISUAL GJ on 28 May 2007 06:34:08.666 UT.

in the cloud-top-level indicates that there was continuous lightning activity in the cloud in the duration of this GJ. Figure 8(*b*) probably shows an upward propagating tip of a bi-polar streamer structure. In figure 8(*c*), this GJ has reached the fully developed stage and optically bridges the cloud top (∼16 km) and the lower ionosphere (∼90 km). Finally, in figure 8(*d*), the optical emissions from the fully developed jet have faded and the tip of the trailing jet reaches an altitude of ∼55 km. The brightness of the brightest pixel (∼2 × 2 km) at the fully developed jet stage is ∼1.6 MR (based on the imager data). The temporally and spatially averaged brightness deduced from the $1PN_2$-filtered imager data is ∼0.6 MR. For the trailing jet, the brightness of the brightest pixel is ∼1.9 MR, and the temporally and spatially averaged brightness is 0.6 MR. The inferred excited numbers of the major nitrogen emission bands and the band percentage to the energy deposition for this event are listed in table 4. The brightness and the excited numbers of the major nitrogen emission bands are lower than those for sprites and elves, as can be seen in table 4. The ratio of the excited number of $2PN_2$ to $1PN_2$ ($N_{2P}/N_{1P} = 0.21$) is similar to that in sprites (section 4.1) and $\Lambda_{\text{total}}/\Lambda_{1P} \sim 10$. The deposited energy for this GJ amounted to only 9.3 MJ, which surprisingly failed to match its spectacular appearance.

5. Discussion

Based on the $1PN_2$-filtered optical data from the ISUAL experiment, the average energy deposition in the upper atmosphere for sprites, halos and elves is deduced to be 22 MJ, 14 MJ and 19 MJ, respectively. However, the total energy deposition in TLEs should also include the energy associated with the formation of minor species at the streamer tip and the other follow-on chemistry reactions. The formation enthalpy of the minor species like $O(^1S)$, $O(^1D)$, $O(^3P)$, $N(^4S)$, $N(^2D)$, $N(^2P)$ [30] is the energy needed to break the chemical bonds of the major species (N_2 and O_2) [44].

As listed in table 2, the electron impact processes with O_2 involve the dissociation of O_2 and the formation of $O(^1D)$ and $O(^3P)$. The formation enthalpies of $O(^1S)$, $O(^1D)$, $O(^3P)$, N are 156.40 kcal mol^{-1}, 104.78 kcal mol^{-1}, 59.533 kcal mol^{-1} and 112.979 kcal mol^{-1}, respectively [44]. If the induced $O(^1D)$ density at the sprite altitude of 70 km is 10^6 cm^{-3} [30], the number of $O(^1D)$ in the sprite volume ($10 \times 10 \times 10$ km^3 = 10^{18} cm^3) is 10^{24} atoms. The quantity of the induced $O(^1D)$ is ∼1.7 mol since a mole is equal to ∼6×10^{23} atoms. The energy required to generate $O(^1D)$ is on the order of $1.7 \times 104.78 \times 10^3 \times 4.1868 \sim 0.75$ MJ, where 1 calorie equals 4.1868 J. However if the induced $N(^2D)$ density at sprite altitude 70 km is 10^7 cm^{-3} [30], then the energy needed to generate $N(^2D)$ is on the order of ∼8 MJ, provided the enthalpy of $N(^2D)$ is approximately the same as the enthalpy of N. Similarly, the energy to dissociate N_2 is also not included in our consideration of the collision processes of electrons on N_2. The energy needed to break up N_2 into N can be as high as 10 MJ in the volume occupied by a sprite. Hence the chemical reaction energy could be up to 50% of that derived

Table 5. The average brightness and the deposited energy for 1415 ISUAL TLEs.

TLE	Average brightness (MR)	Λ_{1P} (MJ)	Λ_{total} (MJ)	Global TLE occurrence rate (per minute)	Global energy deposition rate (MJ min^{-1})
Sprite	1.5 ± 1.1	2.2	22	1	22
Halo	0.3 ± 0.1	1.4	14	1	14
Elve	0.17 ± 0.08	1.9	19	35	665

from ISUAL optical data (22 MJ). The works to compute the energy associated with the chemical reactions in halos and elves are ongoing. However due to higher occurrence altitudes and thus a more rarified ambient atmosphere, they are expected to be substantially lower than that in sprites.

In previous studies [22, 51, 52], the energy deposition in the volume occupied by a sprite can be estimated in three ways: the first method is to compute the electric energy of the quasi-electrostatic field established by the sprite-producing lightning discharge [51, 52]; second, infer the total energy from the observed photonic emissions [52]; third, determine the total energy deposition in the rotational, the vibrational and the other electronic levels for molecular nitrogen and oxygen [22]. The characteristic energy associated with a sprite ranged from ∼1–10 MJ to 1 GJ [22, 52, 53]. To initiate sprites, the lightning quasi-static E-field has to exceed the conventional breakdown value of 240 V m^{-1} at 70 km where breakdown E-field is ∼120 Td, and neutral density is $\sim 2 \times 10^{15}$ cm^{-3} from the MSIS model [47]. Assuming that the energy deposition is almost the same order of magnitude as the electrostatic potential energy associated with the breakdown E-field, the electric energy can be expressed as $\varepsilon_0 E^2 V/2$, where the permittivity in vacuum ε_0 is 8.86×10^{-12} F m^{-1}, the quasi-electrostatic E-field, E, is at least 240 V m^{-1} at 70 km and the volume occupied by a sprite V is about 4×10^{12} m^3 (section 4.1). The electric energy and, therefore, the deposited energy is at least ∼1 MJ in a sprite.

However, one should keep in mind that lightning-induced TLEs are just optical manifestations of the coupling between the troposphere and the upper atmosphere. All the tropospheric lightning activity (both inter-/intra-cloud and CG discharges) should also precipitate a certain amount of energy in the upper atmosphere. At a given second there are ∼50 lightning flashes [54] on the Earth and this translates into nearly 3000 lightning flashes per minute. If on average each flash contributes ∼10% of the energy precipitated by TLEs to the upper atmosphere, the energy transported from the troposphere to the upper atmosphere by the lightning could be up to hundreds of gigajoules per minute.

6. Summary

After three years of observations, ISUAL has recorded only 19 GJs. Hence in this paper, to estimate the global energy deposition we consider only sprites, halos and elves and the results are listed in table 5. We analysed 1415 ISUAL recorded TLEs and found that the spatially averaged brightness inferred from ISUAL images with integration time of 29 ms are 1.5 MR, 0.3 MR and 0.17 MR for sprites, halos and elves, respectively. The averaged energy deposition for the $1PN_2$ band is 2.2, 1.4 and 1.9 MJ for sprites, halos and elves. Therefore the corresponding total energy depositions from all emission bands are 22, 14 and 19 MJ. Since the ISUAL derived global occurrence rates for sprites, halos and elves are 1, 1 and 35 events per minute [32], the energy deposition rates are 22, 14 and 665 MJ min^{-1} for sprites, halos and elves. The total energy precipitation rate in the upper atmosphere due to all the TLEs is estimated to be ∼700 MJ per minute. Since on the Earth there are ∼3000 lightning flashes per minute, the energy precipitation in the upper atmosphere due to lightning activity could be up to two orders of magnitude higher, provided each flash contributes up to 10% of the energy deposited by an elve.

Acknowledgments

Thanks are due to Drs David Sentman and Victor Pasko for fruitful discussions and to Dr Ute Ebert for encouragement. Works performed at NCKU were supported in part by the National Space Center and the National Science Council in Taiwan under grant numbers: 97-NSPO(B)-ISUAL-FA09-01, NSC96-2111-M-008-019, NSC96-2811-M-008-052 and NSC97-2111-M-006-001-MY3.

References

[1] Sentman D D, Wescott E M, Osborne D L, Hampton D L and Heavner M J 1995 Preliminary results from the Sprites94 aircraft campaign: 1. Red sprites *Geophys. Res. Lett.* **22** 1205–8

[2] Boeck W L, Vaughan O H Jr, Blakeslee R, Vonnegut B and Brook M 1992 Lightning induced brightening in the airglow layer *Geophys. Res. Lett.* **19** 99–102

[3] Fukunishi H, Takahashi Y, Kubota M, Sakanoi K, Inan U S and Lyons W A 1996 Elves: lightning-induced transient luminous events in the lower ionosphere *Geophys. Res. Lett.* **23** 2157–60

[4] Barrington-Leigh C P, Inan U S and Stanley M 2001 Identification of sprites and elves with intensified video and broadband array photometry *J. Geophys. Res.* **106** 1741–50

[5] Moudry D, Stenbaek-Nielsen H, Sentman D and Wescott E 2003 Imaging of elves, halos and sprite initiation at 1 ms time resolution *J. Atmos. Sol. Terr. Phys.* **65** 509–18

[6] Pasko V P, Stanley M A, Mathews J D, Inan U S and Wood T G 2002 Electrical discharge from a thundercloud top to the lower ionosphere *Nature* **416** 152–4

[7] Wescott E M, Sentman D, Osborne D, Hampton D and Heavner M 1995 Preliminary results from the Sprites94 aircraft campaign: 2. Blue jets *Geophys. Res. Lett.* **22** 1209–12

[8] Su H T, Hsu R R, Chen A B, Wang Y C, Hsiao W S, Lai W C, Lee L C, Sato M and Fukunishi H 2003 Gigantic jets between a thundercloud and the ionosphere *Nature* **423** 974–6

[9] van der Velde O A, Lyons W A, Nelson T E, Cummer S A, Li J and Bunnell J 2007 Analysis of the first gigantic jet recorded over continental North America *J. Geophys. Res.* **112** 20104

[10] Barrington-Leigh C P, Pasko V P and Inan U S 2002 Exponential relaxation of optical emissions in sprites *J. Geophys. Res.* **107** 1065

[11] Stenbaek-Nielsen H C, Moudry D R, Wescott E M, Sentman D D, Sâo Sabbas F T 2000 Sprites and possible mesospheric effects *Geophys. Res. Lett.* **27** 3829–32

[12] Stenbaek-Nielsen H C, McHarg M G, Kanmae T and Sentman D D 2007 Observed emission rates in sprite streamer heads *Geophys. Res. Lett.* **34** 11105

[13] Kuo C-L *et al* 2007 Modeling elves observed by FORMOSAT-2 satellite *J. Geophys. Res.* **112** 11312

[14] Mende S B, Frey H U, Hsu R R, Su H T, Chen A B, Lee L C, Sentman D D, Takahashi Y and Fukunishi H 2005 D region ionization by lightning-induced electromagnetic pulses *J. Geophys. Res.* **110** 11312

[15] Uman M A 1987 *The Lightning Discharge* (Orlando, FL: Academic)

[16] Barrington-Leigh C P and Inan U S 1999 Elves triggered by positive and negative lightning discharges *Geophys. Res. Lett.* **26** 683–6

[17] Frey H U *et al* 2007 Halos generated by negative cloud-to-ground lightning *Geophys. Res. Lett.* **34** 18801

[18] Hsu R *et al* 2005 Gigantic jet observation by the ISUAL payload of FORMOSAT-2 satellite *AGU Fall Meeting Abstracts* **23** 0992

[19] Armstrong R A, Shorter J A, Taylor M J, Suszcynsky D M, Lyons W A and Jeong L S 1998 Photometric measurements in the SPRITES '95 & '96 campaigns of nitrogen second positive (399.8 nm) and first negative (427.8 nm) emissions *J. Atmos. Sol. Terr. Phys.* **60** 787–99

[20] Suszcynsky D M, Roussel-Dupr R, Lyons W A and Armstrong R A 1998 Blue-light imagery and photometry of sprites *J. Atmos. Sol. Terr. Phys.* **60** 801–9

[21] Hampton D L, Heavner M J, Wescott E M and Sentman D D 1996 Optical spectral characteristics of sprites *Geophys. Res. Lett.* **23** 89–92

[22] Heavner M 2000 Optical spectroscopic observation of sprites, blue jets, and elves *PhD Thesis* University of Alaska-Fairbanks, Fairbanks, AK

[23] Kanmae T, Stenbaek-Nielsen H C and McHarg M G 2007 Altitude resolved sprite spectra with 3 ms temporal resolution *Geophys. Res. Lett.* **34** 07810

[24] Mende S B, Rairden R L, Swenson G R and Lyons W A 1995 Sprite spectra; N_2 1 PG band identification *Geophys. Res. Lett.* **22** 2633–6

[25] Liu N and Pasko V P 2005 Molecular nitrogen LBH band system far-UV emissions of sprite streamers *Geophys. Res. Lett.* **32** 05104

[26] Kuo C-L, Hsu R R, Chen A B, Su H T, Lee L C, Mende S B, Frey H U, Fukunishi H and Takahashi Y 2005 Electric fields and electron energies inferred from the ISUAL recorded sprites *Geophys. Res. Lett.* **32** 19103

[27] Liu N *et al* 2006 Comparison of results from sprite streamer modeling with spectrophotometric measurements by ISUAL instrument on FORMOSAT-2 satellite *Geophys. Res. Lett.* **33** 01101

[28] Enell C F *et al* 2008 Parameterisation of the chemical effect of sprites in the middle atmosphere *Ann. Geophys.* **26** 13–27

[29] Rycroft M J, Odzimek A, Arnold N F, Fullekrug M, Kulak A and Neubert T 2007 New model simulations of the global atmospheric electric circuit driven by thunderstorms and electrified shower clouds: the roles of lightning and sprites *J. Atmos. Sol. Terr. Phys.* **69** 2485–509

[30] Sentman D, Stenbaek-Nielsen H, McHarg M and Morrill J 2008 Plasma chemistry of sprite streamers *J. Geophys. Res.* **113** D11112

[31] Chern J L, Hsu R R, Su H T, Mende S B, Fukunishi H, Takahashi Y and Lee L C 2003 Global survey of upper atmospheric transient luminous events on the ROCSAT-2 satellite *J. Atmos. Sol. Terr. Phys.* **65** 647–59

[32] Chen B *et al* 2008 Global distributions and occurrence rates of transient luminous events *J. Geophys. Res.* **113** A08306

[33] Adachi T *et al* 2006 Electric field transition between the diffuse and streamer regions of sprites estimated from ISUAL/array photometer measurements *Geophys. Res. Lett.* **33** 17803

[34] Raizer Y P 1991 *Gas Discharge Physics* (Berlin: Springer)

[35] Liu N and Pasko V P 2004 Effects of photoionization on propagation and branching of positive and negative streamers in sprites *J. Geophys. Res.* **109** 04301

[36] Morgan W L and Penetrante B M 1990 ELENDIF: a time-dependent Boltzmann solver for partially ionized plasmas *Comput. Phys. Commun.* **58** 127–52

[37] Vallance-Jones A 1974 *Aurora* (Dordrecht: Reidel)

[38] Herzberg G 1950 *Molecular Spectra and Molecular Structure* (New York: Van Nostrand)

[39] Naghizadeh-Kashani A Y, Cressault Y and Gleizes A 2002 Net emission coefficient of air thermal plasmas *J. Phys. D: Appl. Phys.* **35** 2925

[40] Laux C O 1993 Optical diagnostics and radiative emission of air plasmas *PhD Thesis* Mechanical Engineering Department, Stanford University, Stanford, CA

[41] Bucsela E, Morrill J, Heavner M, Siefring C, Berg S, Hampton D, Moudry D, Wescott E and Sentman D 2003 $N_2(B\,^3\Pi_g)$ and $N_2^+(A\,^2\Pi_u)$ vibrational distributions observed in sprites *J. Atmos. Sol. Terr. Phys.* **65** 583–90

[42] Green B D *et al* 1996 Molecular excitation in sprites *Geophys. Res. Lett.* **23** 2161–4

[43] Millikan R C and White D R 1963 Systematics of vibrational relaxation *J. Chem. Phys.* **39** 3209–13

[44] Brasseur G and Solomon S 1986 *Aeronomy of the Middle Atmosphere: Chemistry and Physics of the Stratosphere and Mesosphere* (Dordrecht: Reidel)

[45] Gilmore F R, Laher R R and Espy P J 1992 Franck–Condon factors, r-centroids, electronic transition moments, and Einstein coefficients for many nitrogen and oxygen band systems *J. Phys. Chem. Ref. Data.* **21** 1005–107

[46] Jursa A S 1985 *Handbook of Geophysics and the Space Environment* (Hanscom AFB, MA: Air Force Geophysics Laboratory)

[47] Hedin A E 1991 Extension of the MSIS thermosphere model into the middle and lower atmosphere *J. Geophys. Res.* **96** 1159–72

[48] Verronen P T *et al* 2005 A comparison of night-time GOMOS and MIPAS ozone profiles in the stratosphere and mesosphere *Adv. Space Res.* **36** 958–66

[49] McHarg M G, Stenbaek-Nielsen H C and Kammae T 2007 Observations of streamer formation in sprites *Geophys. Res. Lett.* **34** 06804

[50] Stanley M, Krehbiel P, Brook M, Moore C, Rison W and Abrahams B 1999 High speed video of initial sprite development *Geophys. Res. Lett.* **26** 3201–4

[51] Bering I E A *et al* 2004 The results from the 1999 sprites balloon campaign *Adv. Space Res.* **34** 1782–91

[52] Sentman D D *et al* 2003 Simultaneous observations of mesospheric gravity waves and sprites generated by a midwestern thunderstorm *J. Atmos. Sol. Terr. Phys.* **65** 537–50

[53] Farges T, Blanc E, Le Pichon A, Neubert T and Allin T H 2005 Identification of infrasound produced by sprites during the Sprite2003 campaign *Geophys. Res. Lett.* **32** 01813

[54] Christian H J *et al* 2003 Global frequency and distribution of lightning as observed from space by the Optical Transient Detector *J. Geophys. Res.* **108** 4005